Electronic-structure calculations for polar lattice-structure-mismatched interfaces: PbTe/CdTe(100)

R. Leitsmann* and F. Bechstedt
Institut für Festkörpertheorie und -optik, Friedrich-Schiller-Universität Jena, Max-Wien-Platz 1, 07743 Jena, Germany
(Received 25 April 2007; published 18 September 2007)

The electronic properties of polar interfaces are investigated for the prototypical example of PbTe/CdTe(100) using an *ab initio* pseudopotential method and repeated slab approximations. The band offsets are derived in a two step procedure. Four different methods to calculate an electronic interface band structure are discussed and compared in detail. In contrast to the termination, the lattice-structure mismatch between the PbTe rocksalt and CdTe zinc-blende structure does not play an important role for the position of the Fermi level. In the case of isolated PbTe/CdTe(100) interfaces or layered heterostructures we find a metallic character of the interface band structures. This is explained using a simple ionic model with partially ionized interface atoms. For PbTe/CdTe(100) interfaces with compensating dipole potential a semiconducting band structure is found as a result of fully ionized interface atoms.

DOI: 10.1103/PhysRevB.76.125315 PACS number(s): 68.35.Md, 68.37.Lp, 73.20.At

I. INTRODUCTION

The availability of light sources in the midinfrared spectral region is crucial for many applications, e.g., molecular spectroscopy and gas-sensor systems for environmental monitoring or medical diagnostics. Heiss and co-workers[1] recently demonstrated that PbTe quantum dots (QDs) in a CdTe host matrix exhibit an intense room-temperature midinfrared luminescence. High-resolution transmission electron microscopy (HRTEM) studies[1,2] for the annealed PbTe/CdTe systems have shown the existence of rather ideal PbTe nanocrystals with (111), (100), and (110) interfaces with the CdTe host matrix. There is seemingly an almost lack of asymmetries compared with other QDs prepared by Stranski-Krastanov growth, such as an interconnecting two-dimensional wetting layer, inhomogeneous alloying with the host material, or shape asymmetries.[3] The preceding annealing procedure and the almost vanishing lattice-constant mismatch between PbTe and CdTe suggest a situation for the nanostructured system close to thermal equilibrium. Therefore the shape of these quantum dots can be predicted using parameter-free total energy (TE) calculations.[4]

The theoretical investigation of the tellurides PbTe and CdTe, in particular of their surfaces and interfaces, is a challenging task for different reasons. There is a remarkable ionic contribution to the chemical bonding in PbTe and CdTe. Nevertheless, CdTe has a nonvanishing electron distribution around the Cd-Te connecting line suggesting a directional covalent contribution to its bonds.[5] For PbTe the coordination of the atoms is increased from four to six. As a consequence PbTe crystallizes in rocksalt (RS) structure with the space group $Fm3m$ (O_h^5), whereas the more covalent CdTe crystallizes in zinc-blende (ZB) structure with space group $F\bar{4}3m$ (T_d^2). While a rocksalt (001) surface is nonpolar and hence represents the cleavage face of the crystal, the [001] orientation in the ZB structure leads to a polar (cation-or anion-terminated) surface. In the ZB case the only nonpolar cleavage face is of {110}-type. The different atomic arrangements at the surfaces of the same orientation, but of bulk with a different crystal structure, results in a drastic misfit of the dangling bonds at the interface with respect to position, orientation, and hybridization degree.

The common approximation to describe interfaces between two different materials or even different crystal structures is the repeated-slab (or superlattice) approximation.[6–10] Two thin films are combined to a unit cell along the normal direction. The advantage of the slab approximation is the conservation of a three-dimensional translational symmetry, whereas its disadvantage is the need of the simultaneous treatment of two interfaces, related to one unit cell. Replacing one film by vacuum the repeated-slab approximation is also used to model surfaces.

In the case of electrostatically neutral atomic layers perpendicular to the interface normal, e.g., (110) of zinc blende and (100) as well as (110) of rocksalt, and the same bonding geometry one can construct a symmetric slab with identical interfaces. Band structures and interface energies can be computed for isolated interfaces in this case. Slabs mimicking polar surfaces, e.g., (001) and (111) of zinc blende and (111) of rocksalt, display a net charge in each atomic layer and on the two surfaces themselves. The combination of two polar (or one polar and one nonpolar) stoichiometric slabs leads to a supercell with chemically, structurally, and electrostatically different interfaces, which are denoted by A (cation-terminated) and B (anion-terminated) in the following (100) studies. The different polarities of the two interfaces will introduce a spurious electric field in both material slabs of the supercell, which may affect the electron distribution and the electronic structure. In some cases it is possible to avoid the simultaneous presence of two different A and B faces and to construct symmetric polar slabs with identical interfaces by introducing additional layers consisting of one atomic species.[11] However, such slabs are nonstoichiometric and have to be handled with care.

Several methods to model polar surfaces can be found in the literature. To prevent, for example, the artificial charge transfer through a material slab (caused by the induced electric fields) either inversion-symmetric slabs[12,13] or a passivation of one surface with pseudohydrogen atoms[14] have been proposed for interfaces to the vacuum. The artificial dipole

field in the vacuum region can be prevented using the dipole correction introduced by Neugebauer and Scheffler[15] and corrected by Bengtsson.[16] The price that one has to pay in the case of inversion-symmetric slabs is the increased slab size. Nevertheless, an efficient and correct treatment of polar surfaces (or even interfaces) remains controversial.[13] Hence it is not surprising to find only few attempts to model polar interfaces with *ab initio* methods.[4,17–24] In some of them the treatment of the induced dipole potential remains unclear.[17,18] In others atomic mixing at the interfaces[21–23] or inversion-symmetric slabs[19] are used. To calculate interface energies of isolated polar interfaces we have introduced an extension to the dipole correction of Neugebauer and Scheffler in Ref. 4. However, a detailed discussion of the influence of the induced dipole field on the electronic properties of polar interfaces in various environments is still missing. There is a more direct way for calculating interface (or surface) properties of polar systems. This is the energy-density formalism of Chetty and Martin.[25] Its applicability has been demonstrated in conjunction with Voronoi polyhedra for surface energies of polar semiconductor surfaces.[26] However, because of its complexity the energy-density formalism is so far restricted to small surface unit cells.

In the present paper we discuss a variety of possible slab approximations for polar interfaces between two compounds with different crystal structure, their advantages and their disadvantages. Thereby, we concentrate on the electronic properties of such interfaces. In particular, we compare different theoretical approaches to calculate accurate band structures for polar interfaces, thin films, or layered heterostructures. As model systems we study PbTe/CdTe(100) interfaces.

II. THEORETICAL MODELING

A. Total-energy calculation

We apply the density-functional theory (DFT) within local-density approximation (LDA) as implemented in the Vienna *ab initio* simulation package (VASP).[27,28] Usually, spin polarization is not taken into acount. However, to evaluate the influence of nonscalar relativistic effects, in particular spin-orbit coupling (SOC), we perform test calculations including noncollinear spins.[29] In the case of the heavy elements forming CdTe and PbTe they play an important role. Spin-orbit splittings of the *p*-like valence electrons are in the range of 1 eV. The interaction of the valence electrons with the remaining ions is modeled by pseudopotentials generated within the projector augmented wave (PAW) method.[30] In II-VI and IV-VI semiconductors the outermost occupied *d* states give rise to shallow semicore bands, which contribute essentially to the chemical bonding.[31] Therefore we treat the Cd $4d$ and Pb $5d$ electrons as valence electrons. An energy cutoff of 15 Ry for the plane-wave basis is sufficient to obtain converged structural properties. The total-energy expression contains a Brillouin zone (BZ) integration, which is replaced by a summation over special points of the Monkhorst-Pack (MP) type.[32] For the bulk fcc structures we apply $11\times11\times11$ **k**-point meshes, whereas in the case of repeated-slab systems we use $1\times7\times7$ **k**-point meshes for the different (100) interface slabs with $\sqrt{2}\times\sqrt{2}$ lateral unit cells. The atomic geometries are allowed to relax until the Hellmann-Feynman forces are smaller than 20 meV/Å. The two cubic crystals CdTe and PbTe have nearly the same cubic lattice constant a_0. The mismatch is smaller than 0.4%. Even at the relatively high annealing temperatures of Ref. 1 the different thermal expansion coefficients lead to a thermally induced strain of less than 0.8% with a negligible effect on the electronic band gap.[33] While the small lattice-constant misfit is neglected the lattice-type mismatch is taken into account.

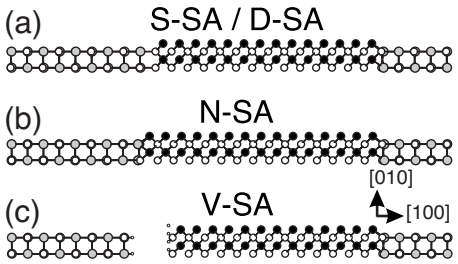

FIG. 1. Schematic stick and ball models of the used four supercells along the [100] direction. Cd: black circles; Pb: gray circles; and Te: white circles; and H^*: tiny white circles. The models are stoichiometric slab approximation (S-SA), dipole-corrected stoichiometric slab approximation (D-SA), nonstoichiometric slab approximation (N-SA), and vacuum slab approximation (V-SA). See text.

B. Slab construction

We compare four different ways to model thin films, isolated interfaces, and layered heterostructures of polar materials. The first model [Fig. 1(a)] contains stoichiometric slabs of the two compounds in one unit cell of their superlattice arrangement without any corrections (S-SA). In this method a superior electric field is induced in each material slab by the periodic boundary conditions, resulting in an (sawtooth-like) electrostatic potential Φ. The difference of its plane-average $\Delta\Phi$ between the left-hand side and the right-hand side of one material slab is independent of the slab size.[4] That means, if one increases the slab thickness, the slope of the dipole potential and thus the resulting forces decrease. Therefore we construct large slabs [28-(bi)layer slabs] to achieve convergence of the atomic displacements with respect to the supercell size. Tests for the (100)PbTe/CdTe system gave no evidence for an interface reconstruction such as $\sqrt{2}\times\sqrt{2}$ (whose cell we widely studied). So, in general, simple 1×1 interface cells are used for the band structure calculations. Because of the equivalence of the anion sublattices in rocksalt and zinc blende, lateral unit cells of the same size and shape can be constructed. A more detailed description can be found in Refs. 4 and 2. The second method, the dipole-corrected stoichiometric slab approximation (D-SA) in Fig. 1(a) applies compensating electric fields. Originally it was introduced to calculate polar interface energies.[4] However, as we will see, this method leads to an electron transfer with respect to the S-SA through the material slabs, whose consequences (for the electronic properties) have to be analyzed in detail. Both approaches, discussed so far, have one

further disadvantage. Due to the periodic boundary conditions always two different interfaces occur in one supercell. The calculated band structures are consequently a mixture of both projected (two-dimensional) interface band structures, i.e., they may contain band states whose localization at one of the two inequivalent interfaces has to be studied carefully.

Symmetric slabs with identical interfaces can easily be constructed by lifting the condition of slab stoichiometry. Thus the third model is the nonstoichiometric slab approximation (N-SA) indicated in Fig. 1(b). Here we introduce an additional Cd layer with respect to the S-SA slab. This results in a supercell with two identical interfaces. Consequently the band structures contain interface bands that are twofold degenerate. The advantage of the model is obvious. Due to the symmetric interfaces we find no superior electric field in this approximation. The disadvantage of this method is the nonstoichiometry. Hence one has to take care of the chemical behavior of the additional layer, and the interface energies depend on the chemical potential μ of the constituents forming this layer. In the fourth method, the vacuum slab approximation (V-SA), shown in Fig. 1(c), we introduce an additional vacuum region in the supercell. In principle, in the V-SA case we use a supercell consisting of three material slabs, PbTe/CdTe/vacuum. The emerging surfaces are passivated with pseudohydrogen atoms to saturate the dangling bonds as known from surface modeling.[14] To passivate the dangling bonds of the fourfold coordinated Te atoms at the CdTe(100)B surface we use pseudohydrogen atoms with a valency of 0.5, which is consistent with the valencies used in Refs. 14 and 34–36 for group VI materials. To passivate the dangling bonds of the sixfold coordinated Pb and Te atoms at the nonpolar PbTe(100) surface we have tested different values for the valancies of the pseudohydrogen atoms. Following the argumentation of Huang *et al.*[36] the optimal passivation is reached for a passivated PbTe cluster with a maximal gap between the highest occupied and the lowest unoccupied orbital. In this way we determined pseudohydrogen valencies of 5/3 and 1/3 to passivate the dangling bonds of the sixfold coordinated Pb and Te atoms, respectively. Interactions across the vacuum region are compensated using the dipole correction introduced by Neugebauer and Scheffler.[15]

The V-SA model seems to be the most promising one to model isolated interfaces because it deals with only one A-or B-terminated interface. However, the price which has to be paid are two additional surfaces, or strictly speaking, two vacuum-material interfaces. Another disadvantage of this approximation is the occurrence of electrostatic dipole fields with a considerable influence on the energetics of the system as we will see later on. A description of the stoichiometric and geometric details are given in Table I and Fig. 1 for all actually used huge supercells.

C. Band-offset determination

To calculate the band offset we use a two-step procedure following the idea of van de Walle and Martin.[37] In order to account for the interface influence, in a first step we calculate the offset between the two different total averages of the electrostatic potential $\Delta(\text{PbTe-CdTe}) = \bar{V}_{\text{CdTe}} - \bar{V}_{\text{PbTe}}$, as schematically indicated in Fig. 2. For this purpose we plot the plane-averaged electrostatic potential (within the interface supercell) along the interface normal. The total average of the electrostatic potential $\bar{V}$ for each material can easily be determined by building the median of the plane-averaged electrostatic potential in the corresponding material slab. To avoid uncertainties arising from the potential slopes in the S-SA and V-SA we compute Δ(PbTe-CdTe) only within the D-SA and N-SA.

TABLE I. Number of atoms and layer thicknesses in Å of the used supercells.

	S-SA	D-SA	N-SA	V-SA
Number of Pb	28	28	28	26
Number of Cd	28	28	30	26
Number of Te	56	56	56	52
Number of pseudo-H	0	0	0	8
Vertical cell size	89.74	89.74	89.74	89.74
Size PbTe	44.87	44.87	43.2675	40.0625
Size CdTe	44.87	44.87	46.4725	40.0625
Size vacuum	0.0	0.0	0.0	9.615

In the second step, the position of the valence band maxima (VBM) in bulk PbTe and bulk CdTe with respect to the averaged electrostatic potential $\bar{V}$ have to be determined. Then the alignment of the averaged potential values Δ(PbTe-CdTe) obtained from the interface calculation leads to the valence band offset (VBO).

With this method we are able to calculate not only the global[56] valence band offset between the L point (VBM of PbTe) and the Γ point (VBM of CdTe) but also some kind of local band offsets at certain $\mathbf{k}$ points. More in detail, the valence band offset is given by

$$\text{VBO}(k_1,k_2) = \text{VBM(PbTe)}(k_1) - \text{VBM(CdTe)}(k_2) - \Delta(\text{PbTe-CdTe}), \quad (1)$$

where $\text{VBM}(k_i)$ is the highest occupied band at the $\mathbf{k}$ point k_i. To obtain the conduction band offset (CBO) we use the gap energies at the corresponding $\mathbf{k}$ points,

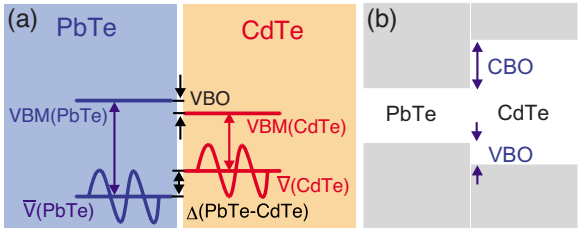

FIG. 2. (Color online) Schematic description of the two-step procedure to calculate the valence band offset (VBO). (a) Determination of the valence-band offset. (b) Schematic picture of the type-I heterostructure obtained at a PbTe-CdTe interface.

TABLE II. Electronic properties of bulk PbTe and CdTe. The gap energies are given in eV and the values of the longitudinal effective electron and hole masses m_l^* of PbTe are given in units of the free electron mass.

		LDA	LDA+SOC	Experiment
Gap	PbTe-L	0.61	0.13	0.19[a]
	CdTe-Γ	0.63	0.34	1.6[a]
m_l^* PbTe	Hole	0.51	1.71	0.31±0.05[b]
	Electron	0.32	0.59	0.24±0.05[b]

[a]References 39 and 40.
[b]Reference 41.

$$\mathrm{CBO}(k_1,k_2) = E_{\mathrm{gap}}^{\mathrm{CdTe}}(k_2) - E_{\mathrm{gap}}^{\mathrm{PbTe}}(k_1) - \mathrm{VBO}(k_1,k_2). \quad (2)$$

Since the VBM is located at the L point for PbTe and at the Γ point for CdTe the global valence band offset is given by

$$\mathrm{VBO} \equiv \mathrm{VBO}(L,\Gamma). \quad (3)$$

The band extrema and the whole band structures are taken from the Kohn-Sham eigenvalues of the DFT-LDA. Since quasiparticle effects[38] have little influence on the relative position of the VBM in common anion materials such as PbTe and CdTe, the excitation aspect is negligible for the alignment procedure and the valence bands. However, this is not true for the position of the conduction bands relative to the valence bands. Therefore we will later apply measured gap values for both PbTe and CdTe to derive the true CBO as indicated in Fig. 2(b).

III. RESULTS AND DISCUSSION

A. Relativistic effects

One expects strong relativistic effects due to the occurrence of heavy elements in the telluride heterostructures under consideration. For electronic properties such as band gaps, effective masses, and similar quantities, this is indeed the case, as can be seen in Table II or in the bulk band structures of PbTe (Fig. 3) and CdTe (Fig. 4). The LDA band gap of PbTe (0.61 eV) at the L point clearly overestimates the experimental value of 0.19 eV[39,40] as a result of the neglected relativistic effects. The inclusion of spin-orbit interaction shrinks the PbTe gap (Table II); but the resulting longitudinal (along $L\Gamma$) effective electron and hole masses m_l^* are much too large compared to the experimental values (Table II). This can be interpreted as an indication for a repulsive interaction between the VBM and CBM band at the L point. An investigation of the band character confirms this suspicion. We observe an interchange of the symmetry character of the VBM and CBM at the L point. In this sense the obtained PbTe gap value of 0.13 eV has to be considered as a negative value. A better description of the electronic states of PbTe near the L point seems to be obtained either by all-electron calculations[42,43] or by starting from a generalized Kohn-Sham scheme using a hybrid functional instead of the LDA for the exchange-correlation (XC) energy of the DFT.[44] However, these electronic structure schemes are computationally very demanding and therefore not suitable for the treatment of interfaces with more than 100 atoms in the supercell.

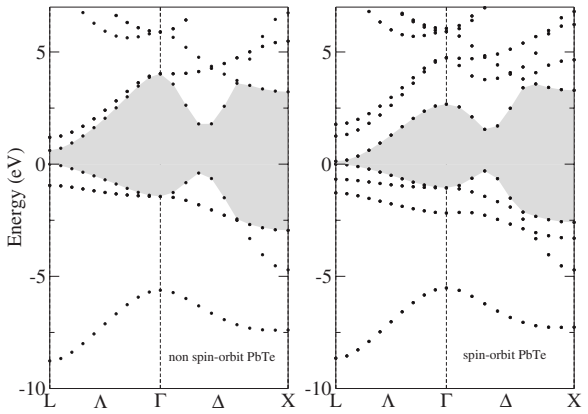

FIG. 3. Calculated electronic band structure of PbTe. Left panel: without spin-orbit effects and right panel: with spin-orbit effects. The top of the valence bands is taken as energy zero.

However, already the DFT-LDA gives a good approximation of the PbTe and CdTe band structures (as shown in Figs. 3 and 4), except of the spin degeneracy and the overestimation of the PbTe-gap value. Therefore we think that the DFT-LDA description can be used for a qualitative discussion of the resulting interface electronic structures within the applied approaches.

B. Band alignment

Using the procedure described in Sec. II C, we obtain a value of Δ(PbTe-CdTe)=2.90 eV for the offset between the total averages of the electrostatic potentials in PbTe and CdTe independent of the used approximation as demonstrated in Fig. 5. The values for the resulting global VBO are given in Table III. To calculate the global CBO with Eq. (2) we have to use the fundamental gap values of PbTe and CdTe. It is well-known that the fundamental gap values are not correctly described in the LDA.[38] Therefore we would

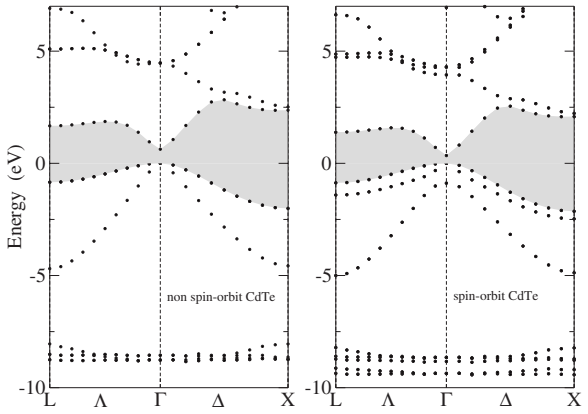

FIG. 4. Calculated electronic band structure of CdTe. Left panel: without spin-orbit effects and right panel: with spin-orbit effects. The top of the valence bands is taken as energy zero.

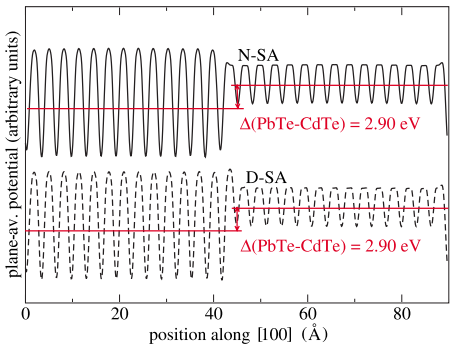

FIG. 5. (Color online) Plane-averaged electrostatic potential along the [100] direction of the supercell in N-SA (top panel) and D-SA (bottom panel). The total averages of the electrostatic potential $\bar{V}_{\mathrm{PbTe}}$ and $\bar{V}_{\mathrm{CdTe}}$ and the difference of both are indicated in red (light gray).

end up with a CBO underestimating the experimental value. Even the character of the heterostructure would change. To bypass these problems related to many-body effects in excited systems and to enhance the comparability with experimental results, we use the experimentally observed gap values of PbTe and CdTe given in Table II to derive CBO from VBO. In this way we obtain a type-I character of the PbTe/CdTe heterostructure.

In Table III we give not only the band offsets of the polar PbTe/CdTe(100) interface, but also the values obtained in Ref. 45 for the nonpolar PbTe/CdTe(110) interface. Since no artificial electrostatic fields are induced at nonpolar interfaces the comparability of the results between both interfaces are an indicator for the quality of our description of polar interfaces. The obtained small variations with respect to the interface orientation are in agreement with the small orientation dependence of the VBO obtained for GaAs/AlAs heterostructures[46] or ZnSe/GaAs, GaAs/Ge, and ZnSe/Ge superlattices.[47] Inclusion of spin-orbit interaction in the calculation leads to nearly vanishing valence band offset so that we expect rather flat hole wells. On the other hand, we observe remarkable offsets for the conduction bands. The trend for the VBO seems to be in agreement with the common anion rule. An estimate for the CBO can be made within the electron affinity rule.[48] Using the electron affinities of 4.3 eV (CdTe)[49] and 4.6 eV (PbTe)[49] a CBO of 0.3 eV is predicted.

TABLE III. Global valence band offsets (VBO) and conduction band offsets (CBO) of the PbTe/CdTe interface for two different interface orientations.

[eV]		(110)[b]	(100)
VBO	LDA	0.42	0.37
CBO[a]	LDA	0.99	1.04
VBO	LDA+SOC	0.05	0.00
CBO[a]	LDA+SOC	1.36	1.41

[a]The conduction-band offset is obtained using experimental gap values.
[b]Reference 45.

This value is of the same order of magnitude as the values given in Table III. However, there is at least an uncertainty of about 0.2 eV in Ref. 49. The resulting gap discontinuity may be 0.2 eV smaller than that in Table III. To our knowledge neither experimental nor theoretical calculations of the PbTe-CdTe VBO exist. However, the VBO and CBO of CdS/PbS (derived from an expression of Nethercot[50]) are estimated to be 0.9 and 1.2 eV, respectively.[51] Taking into account the different fundamental gap values of PbS (0.4 eV)[51] and CdS (2.5 eV)[51] compared to PbTe (0.19 eV) and CdTe (1.6 eV) these values are in good agreement with our predictions. Similar to the studied PbTe/CdTe case very small VBOs of 0.10 ± 0.06 eV have been determined by core-level x-ray photoemission spectroscopy at ZnTe/CdTe(111) heterojunctions.[52]

Up to now we have considered only the global VBO and CBO. Since the VBM and the CBM of PbTe and CdTe are located at different positions in k-space the VBO and CBO can only be directly accessed in experiments allowing for indirect transitions, i.e., in experiments with momentum transfer to the electrons. However, in many experiments, e.g., in zero-phonon photoluminescence measurements or optical absorption spectra only direct transitions are allowed. In such cases local band offsets at certain **k** points have to be considered, which are in general larger than the global offsets.

C. Electrostatics at polar interfaces

To understand the electronic properties of polar interfaces or corresponding layered heterostructures it is instructive to consider a simple ionic model first. We follow a discussion for polar free-standing ZnO slabs.[53] In principle, a purely ionic crystal consists of negatively charged anions and positively charged cations, which build together neutral and nonpolar building blocks as indicated by the blue building blocks in Fig. 6. In such a simple isolator model we find completely occupied bulk valence bands and empty bulk conduction bands as schematically indicated (by shaded and white boxes) in the lower panel of Fig. 6. Such an isolator-like band structure is the result of the fully ionized bulk atoms (we will speak in the following about fully ionized atoms referring to the "bulklike" ions), in the case of a purely ionic model of CdTe: Te^{2-} and Cd^{2+} ions. These ions indeed have only fully occupied or empty sp valence shells with electron configurations $Ar(3d)^{10}(4s)^2(4p)^6(4d)^{10}(Cd^{2+})$ and $Cd^{2+}(5s)^2(6p)^6(Te^{2-})$. At polar surfaces or interfaces the building blocks are not complete anymore, resulting in an excess surface charge σ_{exc} (see red surface building blocks at fully ionized surfaces in Fig. 6). In the case of the CdTe(100) surface we find $-1e$ per ion at the tellurium-terminated B-face of the slab and $+1e$ per ion at the cadmium-terminated A-face of the slab. We will call such surfaces or interfaces "fully ionized." From the Poisson equation it follows that the potential difference between both slab sides $\Delta\Phi$ is directly proportional to the slab thickness d and the surface excess charge σ_{exc}. Since σ_{exc} is independent of the slab size, $\Delta\Phi$ will be divergent in infinitely large slabs, in other words such interfaces/surfaces are unstable. However, the diver-

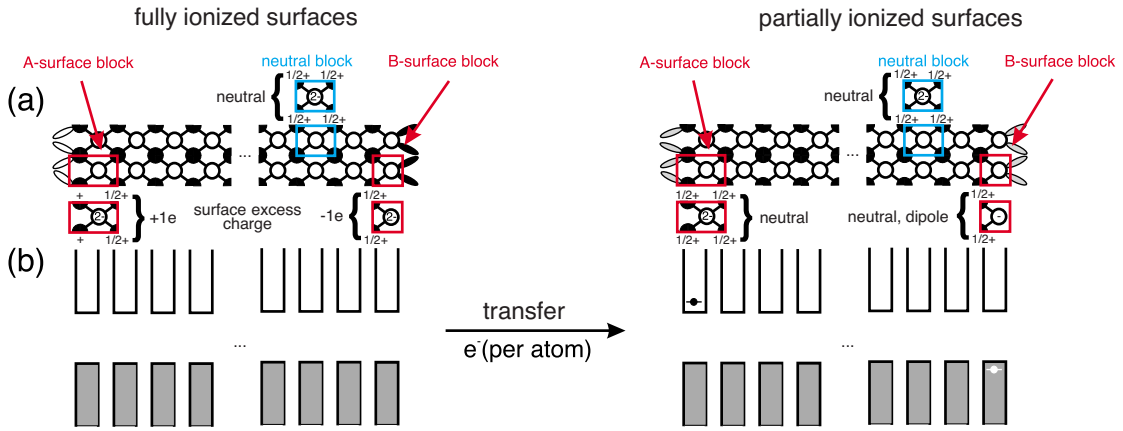

FIG. 6. (Color online) Point-charge picture of the electron distribution in an ionic slab with ZB structure. Two situations, without (left) and with (right) electron transfer (compared to a bulklike electron distrubution) between the A and B surface are sketched. In the upper part (a) we show the arrangements of anions (white balls) and cations (black balls) at A and B surfaces, the building blocks are indicted by red and blue boxes. Half-filled (gray), filled (black), and empty (white) dangling bonds at the surfaces are indicated. The white (shaded) bars in the lower part (b) indicate the local positions of empty conduction (filled valence) bands. The partially occupied conduction (valence) states at partially ionized surfaces are indicated by black (white) circles.

gence of $\Delta\Phi$ can be removed by transferring the excess electrons from the anion side to the cation side of the slab, i.e., by setting σ_{exc} equal to zero. This results in only partially ionized surface/interface atoms. In the case of CdTe(100) we find Te^{-} and Cd^{+} surface ions. The dipole potential of such slabs is constant[54] with respect to the slab thickness d, but nonzero. This is the result of the neutral but polar building blocks (see red surface building blocks at partially ionized surfaces in Fig. 6) at the partially ionized surfaces/interfaces. Using the nonvanishing zero-field polarization P of the material slab we can still define a surface/interface charge density $\sigma_{\mathrm{pol}} \sim P$, which is now inversely proportional to the slab thickness d, leading to a constant potential difference $\Delta\Phi$ with respect to the slab size. In the simple model of partially ionized interfaces/surfaces we find empty valence states (white circle in the valence bands in Fig. 6) at anion-terminated and occupied conduction states (black circle in the conduction bands in Fig. 6) at cation-terminated interfaces/surfaces, which correspond to the half-filled dangling bonds of the interface/surface atoms. This is in contrast to the completely filled valence and conduction states at fully ionized interfaces/surfaces.

The above discussed simple ionic model is just a very rough description of a real CdTe crystal and its polar (100) surfaces. All effects related to the nonvanishing covalent character of CdTe are neglected as well as bonds, which will be formed across the interfaces, or the formation of interface states. Nevertheless this model can describe important effects as we will see in the discussion of the interface band structures below.

D. Band structures

Within the S-SA we have calculated the atomic displacements at PbTe/CdTe(100) interfaces in a previous paper.[4] The relaxation of the atomic positions is important for both the interface energetics and the electronic structure. For the purpose of treating the different slab approaches described in Fig. 1 on the same footings we allow the relaxation of the atomic positions also within the N-SA and V-SA. The good news is, as expected, the results for the atomic displacements with respect to the bulk positions are independent (within an error bar of 0.05 Å) of the actually used slab approach S-SA, N-SA, or V-SA as far as the slab thicknesses are big enough. For the following calculations we have used these relaxed interface geometries to calculate the electronic band structures within the four different slab approaches indicated in Fig. 1.

1. S-SA

In the stoichiometric slab approximation without any electrostatic corrections the induced dipole field Φ leads to differently aligned electronic states at the A and B interfaces. The offset between the VBM at the Cd-terminated and the VBM at the Te-terminated interface can be estimated (from an inspection of the plane average of the electrostatic potential) to 1.7 eV as indicated in the lower part of Fig. 7. Since this value is much larger than the fundamental band gap of PbTe (0.19 eV) a metallic band structure is observed for the studied PbTe/CdTe(100) superlattice (Fig. 7, upper panel). In particular, the state $c\Gamma$, which roughly corresponds to the lowest projected bulk CdTe-CBM, lies below the Fermi level, while the state vJ, which corresponds to the highest projected bulk PbTe-VBM, lies above the Fermi level. Their energy positions are results of the induced potential Φ, which leads to an electron transfer (with respect to the bulk charge distribution) from the VBM at the Te-terminated interface to the CBM at the Cd-terminated interface, as can be seen in Fig. 7. There we have plotted the plane-average of the wave-function squares of two empty valence states $(v\Gamma, vJ)$ and two occupied conduction states $(c\Gamma, cJ)$.

Both valence-derived states above the Fermi-level, $v\Gamma$ and vJ, are localized at the Te-terminated interface, while the two conduction-derived states below the Fermi-level, $c\Gamma$ and

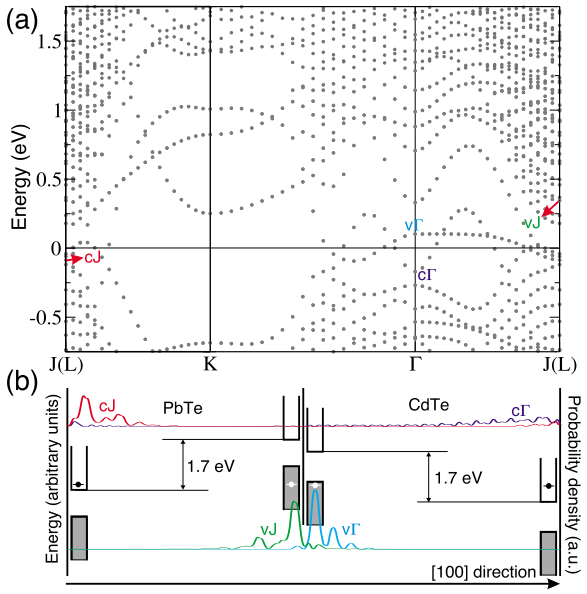

FIG. 7. (Color online) Upper part (a). Band structure of the PbTe/CdTe(100) system within S-SA. The Fermi level is taken as energy zero. Lower part (b). Schematic picture of the electrostatic alignment of the occupied valence states (filled boxes) and the empty conduction states (empty boxes) along the [100] direction. The localization of the plane averaged wave-function squares of selected states indicated in the band structure are shown by the colored curves.

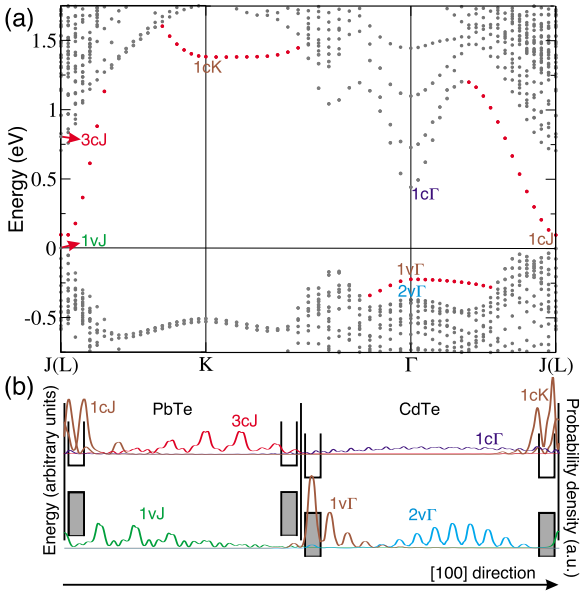

FIG. 8. (Color online) Upper part (a). Band structure of the PbTe/CdTe(100) system within D-SA. The Fermi level is taken as energy zero. Interface states around the Fermi level are shown in red, while states with a bulklike character are shown in gray. Lower part (b). Schematic picture of the electrostatic alignment of the occupied valence states (filled boxes) and the empty conduction states (empty boxes) along the [100] direction. The localization of the plane averaged wave-function squares of selected states indicated in the band structure are shown by the colored curves.

cJ, are localized at the Cd-terminated interface. This behavior can be explained using a modification of the model of the partially ionized polar CdTe(100) surface in Fig. 6 (right panel). At the PbTe/CdTe(100) interfaces not only the CdTe-interface states are partially filled. Although no indications for covalent bonds across the interface could be found,[4] the PbTe-interface states are only partially filled as well. Since the [100] direction is a nonpolar direction in RS-PbTe, the electron transfer (compared to the bulk) through the PbTe slab is entirely the result of the superimposed potential Φ. For these reasons the S-SA cannot be used to accurately model isolated interfaces. On the other hand, since the occurring dipole filled Φ can be considered as a real effect in layered heterostructures or thin films the S-SA is a good approximation to model the electronic structure of such combined systems.

2. D-SA

If we apply the D-SA an electron transfer with respect to the bulk charge distribution through the slab is suppressed. On the other hand, compared to the S-SA we find a charge transfer, which moves electrons from occupied conduction states at one side of the slab to empty valence states at the other side of the slab, i.e., we find no partially charged states near the interfaces as illustrated in Fig. 8. Therefore this approximation provides a better description of the electron distribution in the PbTe slab if one is interested in isolated interfaces. Nevertheless, in the CdTe slab we find a bulklike electron distribution at the interfaces. This corresponds to the electron distribution in the fully ionized interface model (in the simple ionic model of CdTe) in Fig. 6 and is in contrast to the partially ionized interface layers predicted for electrostatic reasons. Nevertheless, the D-SA has one major advantage, the aligned energy bands within one material slab.

In contrast to the S-SA one obtains an almost semiconducting band structure, i.e., completely filled valence states and completely empty conduction states. The highest occupied bulklike state $1vJ$ and the lowest empty bulklike conduction state $3cJ$ are located in the PbTe slab. In the projection of the three-dimensional (3D) fcc-BZ on the two-dimensional (2D) 1×1 surface BZ the L point is projected onto the J point. Hence the $1vJ$ and $3cJ$ states build the projected fundamental energy gap of bulk PbTe. The bulklike $2v\Gamma$ and $1c\Gamma$ states are localized in the CdTe slab and can therefore be associated with the projected bulk CdTe gap. Within the fundamental gap region we find states, e.g., the states $1cK$, $1cJ$, and $1v\Gamma$, which are localized at the PbTe/CdTe(100) interfaces. While the empty $1cJ$ and $1cK$ states are localized at the Cd-terminated interface, the occupied $1v\Gamma$ state is localized at the Te atoms of the Te-terminated interface, as can be seen in Fig. 9, were we have plotted the wave-function square within two different planes perpendicular to the interface.

The shape of $1v\Gamma$ is p-like and it is rotated by 45° compared to the RS-PbTe structure (see Fig. 9, left panel). Therefore it may be written as a linear combination of p_z and p_y orbitals. Such orbital shapes cannot be explained by the oversimplified purely ionic model of PbTe and CdTe. Rather one

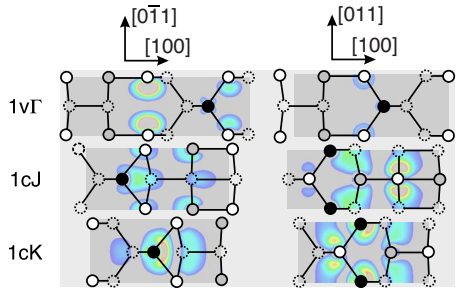

FIG. 9. (Color online) Wave-function square of the states $1v\Gamma$, $1cJ$, and $1cK$ within planes perpendicular to the PbTe/CdTe(100) interface along the $0\bar{1}1$ and [011] direction. High (low) values are indicated by red (blue). The gray regions correspond to regions with almost zero (or rather high) values. The atoms within the plane are represented by white (Te), black (Cd), and gray (Pb) circles. Out of plane atoms are indicated by doted circles.

has to take into account the partially covalent character of CdTe. In this way the shape of $1v\Gamma$ may be explained as the result of a dehybridization of the sp^3-Te orbitals at the Te-terminated PbTe/CdTe(100) interface.[6] The shape of the empty $1cK$ and $1cJ$ states cannot so easily be attributed to single atomic orbitals. They are mainly localized in the region between the Cd, Te, and Pb atoms at the Cd-terminated interface (see Fig. 9). The strong dispersion along the JK and ΓJ directions is the result of a strong interaction of these states along the [011] and [$0\bar{1}1$] directions. On the other hand, along the [001] and [010] directions we observe only a week interaction according to the small dispersion along $K\Gamma$. For the formation of covalent bonding or antibonding states across the interface we found no indications, which is in agreement with the results of Ref. 4. The shape of the states $1cK$ and $1cJ$ rather indicate a nondirectional electrostatic interaction across the PbTe/CdTe(100) interface.

Since the D-SA models fully ionized isolated interfaces with a compensating dipole potential, it is not suitable for the simulation of real isolated interfaces, which should exhibit only partially ionized interface atoms for electrostatic reasons. On the other hand, the D-SA may be used to model systems in which electrostatic fields are forbidden for symmetry reasons, e.g., in highly symmetric PbSe nanocrystals with pairwise occurrence of A and B surface facets on the cubo-octahedral shape.[55]

3. N-SA

In the framework of the N-SA [Fig. 1(b)] the supercell contains symmetric slabs with remarkable consequences for the electronic states. In this approximation, no dipole potential can appear for symmetry reasons. Another advantage of this approach is the occurrence of two identical interfaces, which allows us to compute single interface band structures (in contrast to the former two approximations).

In Fig. 10 we present the obtained N-SA band structure, which has many similarities with the D-SA one (Fig. 8). They concern the projected bulk band structures and the interface bands within the fundamental gap region. However, there are also drastic consequences of the additional Cd

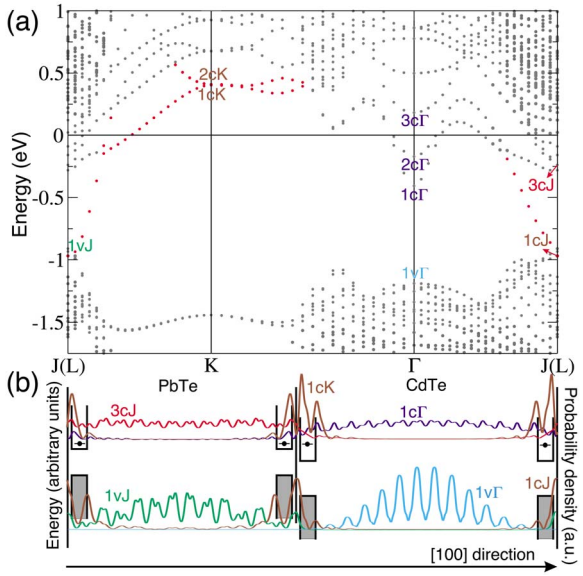

FIG. 10. (Color online) Upper part (a). Band structure of the PbTe/CdTe(100) system within N-SA. The Fermi level is taken as energy zero. Interface states around the Fermi level are shown in red, while states with a bulklike character are shown in gray. Lower part (b). Schematic picture of the electrostatic alignment of the occupied valence states (filled boxes) and the empty conduction states (empty boxes) along the [100] direction. The localization of the plane averaged wave-function squares of selected states indicated in the band structure are shown by the colored curves.

layer. The main differences to the findings in Fig. 8 are the different positions of the Fermi level and the vanishing gap between the $1cJ$ interface state and the PbTe VBM ($1vJ$). Since the slab within the N-SA contains only Cd-terminated interfaces the interface state $1v\Gamma$ of the D-SA model, which is located at a Te-terminated PbTe/CdTe(100) interface, cannot be found in the N-SA band structure. The increased position of the Fermi level in the N-SA is the result of the partially ionized Cd interface atoms. In comparison to the bulk Cd ions they provide more valence electrons. Therefore the interface state $1cJ$ as well as the bulk PbTe and CdTe conduction states, which are energetically close, will be occupied by those electrons (see Fig. 10). In contrast to the S-SA the occupied bulk conduction states are not localized at one interface anymore. Rather they are localized in the whole material slab, as demonstrated in Fig. 10 (lower part). This is a consequence of the vanishing dipole potential Φ within the N-SA.

Comparing the N-SA and D-SA band structures, one may ask oneself if the obtained metallic character of the N-SA band structure is just an artifact of the additional metal layer in its description. Indeed, this is not the case, because locally the stoichiometry is always conserved and therefore no metallic bonding arrangements can be formed. The only artifact of the additional Cd layer is the twofold degeneracy of the interface states $1cK$ and $2cK$. Therefore this approach can be used to accurately calculate band structures of isolated polar interfaces, or of layered heterostructures with identical interfaces. The illustrated situation may also occur in the case

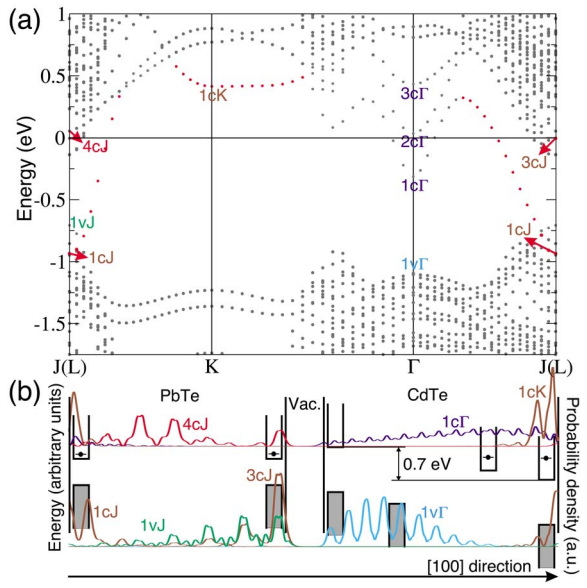

FIG. 11. (Color online) Upper part (a). Band structure of the PbTe/CdTe(100) system within V-SA. The Fermi level is taken as energy zero. Interface states around the Fermi level are shown in red, while states with a bulklike character are shown in gray. Lower part (b). Schematic picture of the electrostatic alignment of the occupied valence states (filled boxes) and the empty conduction states (empty boxes) along the [100] direction. The localization of the plane averaged wave-function squares of selected states indicated in the band structure are shown by the colored curves.

of embedded nanocrystals. In this case, nonstoichiometric stacking of atomic layers seems to be more likely.

4. V-SA

The bonding and antibonding states of the H^*–Cd, H^*–Te, and H^*–Pb bonds at the passivated surfaces are energetically far away from the fundamental gap region. Consequently they do not influence the interface states. Hence we are able to compute band structures of isolated interfaces in the V-SA as well as in the N-SA. However, we still have to deal with a dipole potential, which is induced in the polar CdTe slab and, hence, with a somewhat incorrect energy alignment of the bulklike CdTe states (at least if we are interested in isolated interfaces). This effect is schematically shown in the lower part of Fig. 11.

The potential difference between both sides of the CdTe slab can be estimated from an inspection of the plane-averaged electrostatic potential to a value of 0.7 eV. The influence of this potential on the energetic positions of the electronic states is visible from a comparison of the N-SA and V-SA band structures (Figs. 10 and 11). Both figures exhibit the same general features, e.g., the surface states $1cK$ and $1cJ$ at the PbTe/CdTe(100)-B interface. Again this indicates that the additional Cd-layer in the N-SA is not responsible for the metallic character of the obtained band structure. In fact the metallic character is rather a characteristic feature of the PbTe/CdTe(100)-B interface. The main difference between the N-SA and V-SA band structures, however, is the energetic position of the CdTe bulklike states, e.g., $1c\Gamma$, $2c\Gamma$, or $3c\Gamma$. They are shifted to somewhat higher energies as a result of the electrostatic potential in the CdTe slab. Furthermore, some states, e.g., $3cJ$, are localized at the passivated PbTe surface. Since these surface resonances have a strong bulklike character and do not occur within the fundamental gap region, one can neglect their influence on the remaining band structure.

The additional vacuum region and the remaining dipole field within the polar material slab makes the V-SA an approximation of second choice for the modeling of isolated interfaces as well as for the modeling of layered heterostructures. However, it may be useful to clarify the influence of additional material layers, which have to be introduced in the N-SA.

IV. SUMMARY AND CONCLUSIONS

We have developed four different slab approximations S-SA, D-SA, N-SA, and V-SA to describe polar PbTe/CdTe(100) interfaces. They vary with respect to additional dipole potentials, atomic layers, or vacuum layers.

First, we have calculated the valence and conduction band offsets at the PbTe/CdTe interfaces within the density functional theory in local density approximation. The results are independent from the used approximation (at least for D-SA and N-SA the results are the same) and yield a type-I character of the considered heterostructures applying the experimental gap values of PbTe and CdTe independent of the inclusion or negligence of spin-orbit interaction. Only a weak dependence on the interface orientation is found.

Second, we have discussed the advantages and disadvantages of the four studied slab approximations. To calculate band structures of realistic systems like isolated interfaces or layered heterostructures one has to take care about the correct description of the electrostatic potentials and the ionization degree of the interface atoms. For example, at isolated polar interfaces one expects partially ionized interface atoms for electrostatic reasons. In addition, the slope of the electrostatic potential Φ should vanish since isolated interfaces correspond to infinitely large slabs. Therefore the most reliable results for band structures of isolated interfaces are obtained using the N-SA or V-SA. On the other hand at polar layered heterostructures, superlattices, or in thin films one should be able to find a finite slope of the potential Φ. In general in all systems with a finite slab size the potential Φ can be considered as a real effect and may therefore be modeled by the S-SA. To model interfaces/surfaces of systems where electrostatic fields are forbidden for symmetry reasons, e.g., PbSe nanodots, one has to introduce a compensation field, like in the D-SA. In such cases fully ionized interfaces/surfaces may be stable as well.

Important effects obtained at the band structures of PbTe/CdTe(100) interfaces, which we have used as a prototypical example to account for lattice-structure mismatch, can be explained using a simple ionic model. For example, the shift of the Fermi level towards the PbTe and CdTe conduction states at PbTe/CdTe(100)-B interfaces is the result of the partially ionized Cd-interface ions. In addition we found strongly localized states at PbTe/CdTe(100)-A and -B

interfaces. One of these interface states, namely the $1cJ$ state at the Cd-terminated PbTe/CdTe(100) interface, closes the fundamental gap. Consequently we predict a metallic character for isolated PbTe/CdTe(100)-B interfaces. In other systems, e.g., embedded PbTe nanocrystals in a CdTe matrix internal electrostatic fields may be forbidden for symmetry reasons. In such cases a semiconducting PbTe/CdTe(100) interface band structure can be predicted according to the D-SA. Our studies show that in dependence on geometry and stoichiometry long-range electrostatic fields may significantly influence the local electronic structure of interfaces and heterostructures.

ACKNOWLEDGMENTS

We acknowledge valuable discussions with F. Schäffler (Linz) and colleagues of our group L.E. Ramos, J. Furthmüller, and F. Fuchs. The work was financially supported through the Fonds zur Förderung der Wissenschaftlichen Forschung (Austria) in the framework of SFB25, Nanostrukturen für Infrarot-Photonik (IR-ON), and the EU NANOQUANTA network of excellence Grant No. (NMP4-CT-2004-500198). Grants of computer time from the Höchstleistungsrechenzentrum Stuttgart are gratefully acknowledged.

*roman@ifto.physik.uni-jena.de

[1] W. Heiss, H. Groiss, E. Kaufmann, M. Böberl, G. Springholz, F. Schäffler, K. Koike, H. Harada, and M. Yano, Appl. Phys. Lett. **88**, 192109 (2006).
[2] R. Leitsmann, L. E. Ramos, F. Bechstedt, H. Groiss, F. Schäffler, W. Heiss, K. Koike, H. Harada, and M. Yano, New J. Phys. **8**, 317 (2006).
[3] J. Stangl, V. Holy, G. Bauer, and C. B. Murray, Rev. Mod. Phys. **76**, 725 (2004).
[4] R. Leitsmann, L. E. Ramos, and F. Bechstedt, Phys. Rev. B **74**, 085309 (2006).
[5] J. P. Walter and M. L. Cohen, Phys. Rev. B **4**, 1877 (1971).
[6] F. Bechstedt, *Principles of Surface Physics* (Springer-Verlag, Berlin, 2003).
[7] M. C. Payne, M. P. Teter, D. C. Allan, T. A. Arias, and J. D. Joannopoulos, Rev. Mod. Phys. **64**, 1045 (1992).
[8] L. Quiroga, A. Camacho, L. Brey, and C. Tejedor, Phys. Rev. B **40**, 3955 (1989).
[9] W. R. L. Lambrecht, B. Segall, and O. K. Andersen, Phys. Rev. B **41**, 2813 (1990).
[10] C. Raffy, J. Furthmüller, and F. Bechstedt, J. Phys.: Condens. Matter **14**, 12725 (2002).
[11] J. Goniakowski and C. Noguera, Phys. Rev. B **60**, 16120 (1999).
[12] E. Kaxiras, Y. Bar-Yam, J. D. Joannopoulos, and K. C. Pandey, Phys. Rev. B **35**, 9625 (1987).
[13] S. Mankefors, Phys. Rev. B **59**, 13151 (1999).
[14] K. Shiraishi, J. Phys. Soc. Jpn. **59**, 3455 (1990).
[15] J. Neugebauer and M. Scheffler, Phys. Rev. B **46**, 16067 (1992).
[16] L. Bengtsson, Phys. Rev. B **59**, 12301 (1999).
[17] E. Tarnow, J. Appl. Phys. **77**, 6317 (1995).
[18] R. B. Capaz, H. Lim, and J. D. Joannopoulos, Phys. Rev. B **51**, 17755 (1995).
[19] S. Tanaka and M. Kohyama, Phys. Rev. B **64**, 235308 (2001).
[20] C. Raffy, J. Furthmüller, J. M. Wagner, and F. Bechstedt, Phys. Rev. B **70**, 195344 (2004).
[21] J. von Pezold and P. D. Bristowe, J. Mater. Sci. **40**, 3051 (2005).
[22] W. A. Harrison, E. A. Kraut, J. R. Waldrop, and R. W. Grant, Phys. Rev. B **18**, 4402 (1978).
[23] A. Kley and J. Neugebauer, Phys. Rev. B **50**, 8616 (1994).
[24] M. Städele, J. A. Majewski, and P. Vogl, Phys. Rev. B **56**, 6911 (1997).
[25] N. Chetty and R. M. Martin, Phys. Rev. B **45**, 6074 (1992); **45**, 6089 (1992).
[26] K. Rapcewicz, B. Chen, B. Yakobson, and J. Bernholc, Phys. Rev. B **57**, 7281 (1998).
[27] G. Kresse and J. Furthmüller, Comput. Mater. Sci. **6**, 15 (1996).
[28] G. Kresse and J. Furthmüller, Phys. Rev. B **54**, 11169 (1996).
[29] D. Hobbs, G. Kresse, and J. Hafner, Phys. Rev. B **62**, 11556 (2000).
[30] G. Kresse and D. Joubert, Phys. Rev. B **59**, 1758 (1999).
[31] S.-H. Wei and A. Zunger, Phys. Rev. B **37**, 8958 (1988).
[32] H. J. Monkhorst and J. D. Pack, Phys. Rev. B **13**, 5188 (1976).
[33] J. W. Tomm, L. Werner, D. Genzow, K. Herrmann, D. Schikora, and J. Griesche, Phys. Status Solidi A **106**, 509 (1988).
[34] L.-W. Wang and J. Li, Phys. Rev. B **69**, 153302 (2004).
[35] S. Gundel, A. Fleszar, W. Faschinger, and W. Hanke, Phys. Rev. B **59**, 15261 (1999).
[36] X. Huang, E. Lindgren, and J. R. Chelikowsky, Phys. Rev. B **71**, 165328 (2005).
[37] C. G. Van de Walle and R. M. Martin, Phys. Rev. B **35**, 8154 (1987).
[38] W. G. Aulbur, L. Jonsson, and J. W. Wilkins, *Solid State Physics: Advances in Research and Applications* (Academic, San Diego, 2000), Vol. 54, Chap. Quasiparticle calculations in solids, p. 1.
[39] P. Dziawa, B. Taliashvili, W. Domuchowski, L. Kowalczyk, E. Lusakowska, A. Mycielski, V. Osinniy, and T. Story, Phys. Status Solidi C **2**, 1167 (2005).
[40] S.-H. Wei and A. Zunger, Phys. Rev. B **55**, 13605 (1997).
[41] G. Martinez, M. Schlüter, and M. L. Cohen, Phys. Rev. B **11**, 651 (1975).
[42] E. A. Albanesi, E. L. P. y Blanca, and A. G. Petukhov, Comput. Mater. Sci. **32**, 85 (2005).
[43] E. A. Albanesi, C. M. I. Okoye, C. O. Rodriguez, E. L. Peltzer y Blanca, and A. G. Petukhov, Phys. Rev. B **61**, 16589 (2000).
[44] K. Hummer, A. Grüneis, and G. Kresse, Phys. Rev. B **75**, 195211 (2007).
[45] R. Leitsmann, L. E. Ramos, F. Bechstedt, H. Groiss, F. Schäffler, W. Heiss, K. Koike, H. Harada, and M. Yano, Appl. Surf. Sci. (to be published).
[46] A. Baldereschi, S. Baroni, and R. Resta, Phys. Rev. Lett. **61**, 734 (1988).
[47] R. Eppenga, Phys. Rev. B **40**, 10402 (1989).
[48] R. L. Anderson, Solid-State Electron. **5**, 341 (1962).
[49] S. Movchan, F. Sizov, and V. Tetyorkin, Semicond. Phys., Quantum Electron. Optoelectron. **2**, 84 (1999).
[50] A. H. Nethercot, Phys. Rev. Lett. **33**, 1088 (1974).

[51] J. W. Haus, H. S. Zhou, I. Honma, and H. Komiyama, Phys. Rev. B **47**, 1359 (1993).

[52] T. M. Duc, C. Hsu, and J. P. Faurie, Phys. Rev. Lett. **58**, 1127 (1987).

[53] G. Kresse, O. Dulub, and U. Diebold, Phys. Rev. B **68**, 245409 (2003).

[54] P. W. Tasker, J. Phys. C **12**, 4977 (1979).

[55] K. S. Cho, D. V. Talapin, W. Gaschler, and C. B. Murray, J. Am. Chem. Soc. **127**, 7140 (2005).

[56] Here with "global VBO" the VBO between the VBMs of both materials is meant, while with "local VBO" the VBO between both materials at certain **k**-points is meant.